THE JOURNAL OF PHYSICAL CHEMISTRY A

Article

pubs.acs.org/JPCA

N−H Stretching Modes of Adenosine Monomer in Solution Studied by Ultrafast Nonlinear Infrared Spectroscopy and Ab Initio Calculations

Christian Greve,[†] Nicholas K. Preketes,[‡] Rene Costard,[†] Benjamin Koeppe,[†] Henk Fidder,[†] Erik T. J. Nibbering,*[,†] Friedrich Temps,[§] Shaul Mukamel,[‡] and Thomas Elsaesser[†]

[†]Max-Born-Institut für Nichtlineare Optik und Kurzzeitspektroskopie, Max-Born-Strasse 2 A, D-12489 Berlin, Germany

[‡]Department of Chemistry, University of California, Irvine, California 92697-2025, United States

[§]Institut für Physikalische Chemie, Christian-Albrechts-Universität zu Kiel, Olshausenstrasse 40, D-24098 Kiel, Germany

ABSTRACT: The N−H stretching vibrations of adenine, one of the building blocks of DNA, are studied by combining infrared absorption and nonlinear two-dimensional infrared spectroscopy with ab initio calculations. We determine diagonal and off-diagonal anharmonicities of N−H stretching vibrations in chemically modified adenosine monomer dissolved in chloroform. For the single-quantum excitation manifold, the normal mode picture with symmetric and asymmetric NH_2 stretching vibrations is fully appropriate. For the two-quantum excitation manifold, however, the interplay between intermode coupling and frequency shifts due to a large diagonal anharmonicity leads to a situation where strong mixing does not occur. We compare our findings with previously reported values obtained on overtone spectroscopy of coupled hydrogen stretching oscillators.

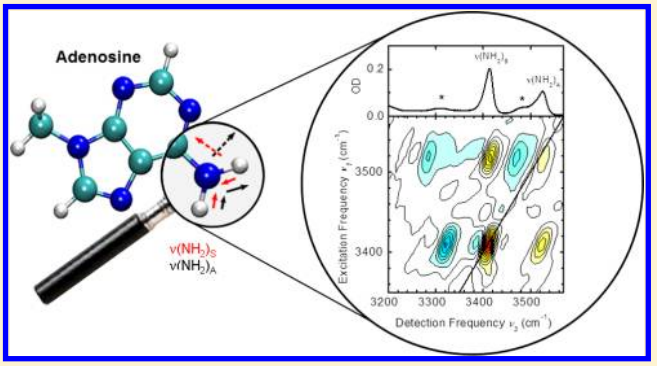

1. INTRODUCTION

Nucleic acid bases, building blocks of DNA and RNA, have been investigated with numerous experimental and theoretical methods. In light of the hydrogen-bonding interactions between complementary nucleic acid bases, linear vibrational spectroscopy has been one of the favored techniques as N−H stretching modes provide a direct local probe of these interactions. Typically, one follows either a top-down approach, where a DNA (or RNA) double helix formed by a specific base pair sequence is studied,[1−3] or a bottom-up approach, where only a limited number of building blocks, that is, nucleic acid bases, are included in the study. In recent years, individual bases and base pairs have been studied in the gas phase[4−7] and in solution.[8−12] Despite the fact that both in the gas phase and in solution such a bottom-up approach involves the existence of several different hydrogen-bonded complexes, a characterization of infrared (IR) spectra has been possible by applying a comparison to theoretical spectra resulting from quantum chemical calculations.

Until now, most of these studies have relied on linear IR spectra that give insight into the frequencies and cross sections of the fundamental $\nu = 0-1$ transitions. Apart from leaving much ambiguity in the assignment of N−H stretching bands, the diagonal anharmonicities and the couplings between different modes, that is, the off-diagonal anharmonicities, have remained unspecified. Ultrafast nonlinear pump−probe and two-dimensional (2D) infrared spectroscopy give direct insight into such behavior, as has been demonstrated for N−H and C═O stretching excitations of DNA sequences and oligomers.[2,3,13−19] To a lesser extent, nucleobase pairs and monomers in solution[12,20−22] have been studied by such techniques. As a result, the diagonal and off-diagonal anharmonicities of uncomplexed nucleic bases have so far remained elusive.

In this article, the N−H stretching modes of adenosine monomer in chloroform solution (Figure 1) are studied by a combination of ultrafast nonlinear infrared spectroscopy and ab initio calculations of vibrational modes and couplings. The adenosine monomer contains an NH_2 group with two local N−H stretching oscillators. We deduce from linear and 2D-IR spectra the diagonal and off-diagonal anharmonicities of the N−H stretching modes. We analyze the observed frequency shifts in the linear and 2D-IR spectra using both normal and local mode representations, the latter allowing for a detailed comparison with theory. We substantiate these results by ab initio calculations, which provide local diagonal anharmonicities and intermode couplings.

Received: April 21, 2012
Revised: June 11, 2012
Published: June 23, 2012

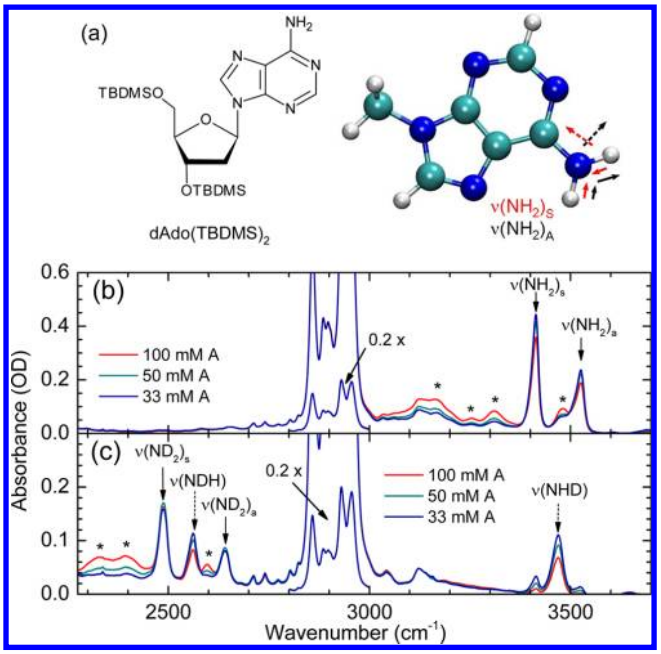

Figure 1. (a) Molecular structure of the A, including the TBDMS-ribose side group. The symmetric and asymmetric N−H stretching normal modes of 9-mA are also shown (solid arrows: nuclear displacements; dashed arrows: dipole moments). (b) Normalized linear FT-IR spectrum of A in $CDCl_3$. (c) Normalized linear FT-IR spectrum of partially H/D-exchanged A in $CDCl_3$. Relevant N−H and N−D stretching modes are assigned with arrows; asterisks denote bands of A···A complexes; the spectral region between 2800 and 3000 cm^{-1} showing the C−H stretching modes of the TBDMS-ribose side groups have been scaled by a factor of 0.2.

2. EXPERIMENTAL AND THEORETICAL METHODS

Linear and Nonlinear IR Spectroscopy. Chemically modified 2′-deoxyadenosine nucleoside was synthesized in a similar fashion as reported before.[11] To increase the solubilities in weakly polar solvents, the hydroxyl groups of the ribose units were substituted with *tert*-butyldimethylsilyl (TBDMS) groups. We denote the chemically modified nucleic base 3′,5′-TBDMS protected 2′-deoxyadenosine as species A (Figure 1a). $CHCl_3$ (Uvasol, ≥99.0% purity) was obtained from Aldrich and $CDCl_3$ from Deutero. The solvent was dried over molecular sieves with pore diameters of 0.3 nm. Deuteration of the amino group of adenosine was obtained by dissolving A in a 100-fold excess amount of methanol-d_1. After a few minutes, the solvent was removed in vacuum. This procedure was repeated once before the substance was taken up in chloroform and the solution was transferred to a cuvette, leading to about a 70% degree of deuteration.

Linear IR spectra were recorded at room temperature with a Varian 640 FT-IR spectrometer (resolution = 1 cm^{-1}). The solutions were held between 1 mm CaF_2 windows with absorption path lengths of 0.2 mm using Teflon spacers. Femtosecond IR pump−probe and 2D-IR photon echo experiments were performed as described before.[12] In short, the mid-IR pulses, generated by parametric down-conversion of the output of an amplified Ti:sapphire laser system, had a center frequency of 3350 cm^{-1} and a pulse energy of 500 nJ; the pulse duration was 50 fs. In the pump−probe experiments, the probe pulses were spectrally dispersed after interaction with the sample (resolution = 4 cm^{-1}). The 2D-IR spectra have a resolution of 10 cm^{-1} along the excitation frequency ν_1 and of 9 cm^{-1} along the detection frequency ν_3. For the ultrafast experiments, we used a 0.04 M solution of A in $CHCl_3$, which was held between 1 mm CaF_2 windows with an absorption path length of 0.2 mm.

Quantum Chemical Calculations. Ab initio calculations were performed on 9-methyladenine (9-mA) and 9-methyladenine-d_2 (9-mA-d_2), where the amino hydrogens have been exchanged with deuterium. All calculations were performed in the gas phase, at the HF/6-311++G** level of theory using Gaussian 09.[23] Linear absorption and absorptive 2D-IR spectra ($k_I + k_{II}$) were calculated using the sum-over-states expressions as implemented in SPECTRON.[24] All calculations were performed in the impulsive limit using a homogeneous dephasing of 4 cm^{-1}. For the 2D-IR calculations, the sum-over-states expressions were used (for a complete description, see ref 25) with the population time (t_2) fixed to 0 fs. To account for inhomogeneous broadening, a stochastic Gaussian frequency fluctuation was added to the symmetric $[(\langle\omega_S^2\rangle - \langle\omega_S\rangle^2)^{1/2} = 21\ cm^{-1}]$ and asymmetric $[(\langle\omega_A^2\rangle - \langle\omega_A\rangle^2)^{1/2} = 30\ cm^{-1}]$ fundamental (eigenstate) frequencies over 500 snapshots.[24] Anharmonic shifts were fixed to the gas-phase values.

3. EXPERIMENTAL RESULTS AND DISCUSSION

Figure 1 shows the linear FT-IR spectra of A in chloroform, before and after partial H/D exchange of the hydrogen atoms in the adenosine NH_2 group. In a normal mode picture, the infrared band of nondeuterated A at 3413 cm^{-1} is assigned to the symmetric NH_2 stretching mode $\nu(NH_2)_S$, while the asymmetric stretching band $\nu(NH_2)_A$ occurs at 3525 cm^{-1}. From the frequency difference between these two transitions, that is, $2J_H = \nu(NH_2)_S - \nu(NH_2)_A = -112\ cm^{-1}$, a "mechanical" coupling of $J_H = -56.0\ cm^{-1}$ between the two local N−H stretching modes can be deduced. Slightly larger values for J_H of −57.5 to −59.0 cm^{-1} are found for gas-phase 9-H-adenine and 9-mA,[26−28] 9H-adenine in helium nanodroplets[6] and in Ar matrixes,[29] and 9-ethyladenine in $CDCl_3$ solution.[8]

In the partially H/D-exchanged sample, the symmetric ND_2 stretching mode $\nu(ND_2)_s$ is observed at 2489 cm^{-1}, and the asymmetric ND_2 stretching mode $\nu(ND_2)_A$ is at 2639 cm^{-1}, leading to a value for the splitting of $2J_D = \nu(ND_2)_S - \nu(ND_2)_A = -154\ cm^{-1}$, that is, $J_D = -77.0\ cm^{-1}$. The H/D exchange yield is estimated to be ∼70%, with the result that not only A monomers with fully exchanged ND_2 groups contribute to the spectrum but also partially exchanged A monomers, for which both the local N−H and the N−D stretching modes of an NHD group are observed. This partial exchange allows determination of the transition frequencies of the virtually decoupled local N−H and N−D stretching modes of the NHD-group, $\nu(NH) = 3469\ cm^{-1}$ and $\nu(ND) = 2565\ cm^{-1}$. These values lie perfectly halfway between the symmetric and asymmetric normal mode stretching frequencies, showing that the exchange of a single hydrogen atom with a deuterium effectively decouples the two local N−H stretching modes. Moreover, it explicitly confirms the validity of regarding the normal modes as linear combinations of the local N−H(D) modes, with a splitting caused by the extracted couplings. From the decoupled local mode frequencies, it follows that the H/D isotope effect on the local NH stretching mode frequency is equal to 1.352, whereas the isotope effect on the coupling between the two local modes is $J_H/J_D = (1.375)^{-1}$.

To determine the vibrational population dynamics, we performed time- and frequency-resolved pump−probe meas-

dx.doi.org/10.1021/jp303864m | J. Phys. Chem. A 2012, 116, 7636−7644

urements. In Figure 2a, transient pump−probe spectra are plotted for delay times between 0.2 and 40 ps. On the

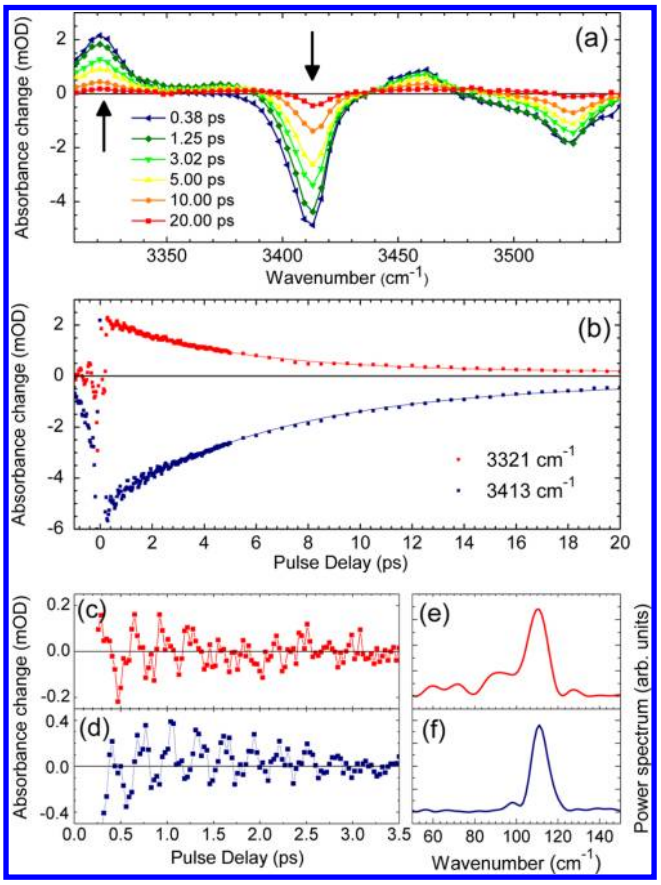

Figure 2. Pump−probe results for A dissolved in $CHCl_3$ (concentration of 40 mM). (a) Transient pump−probe spectra for different delay times. (b) Kinetic traces of signals (symbols) in the range of the symmetric NH_2 stretching mode $\nu(NH_2)_S$ for $\nu = 1-2$ excited-state absorption at 3321 cm^{-1} and the $\nu = 0-1$ absorption decrease at 3413 cm^{-1}. The solid lines represent a single-exponential fit with a 6 ± 1 ps time constant, with the $\nu = 1$ lifetime. (c,d) Oscillatory components of the pump−probe signals and (e,f) respective Fourier transforms showing the 112 cm^{-1} beat frequency.

fundamental transitions at $\nu(NH_2)_S \approx 3415$ cm^{-1} and $\nu(NH_2)_A \approx 3525$ cm^{-1}, one observes a prominent decrease of absorption that is due to the depletion of the respective $\nu = 0$ ground state and stimulated emission from the respective $\nu = 1$ state. The bleaching components below 3380 and 3500 cm^{-1} are caused by transitions of complexed A molecules (cf. asteriks in Figure 1a). The complexed molecules that will not be considered in the following, show a somewhat higher transition dipole μ_t than the (monomeric) species A. Thus, their relative intensity in the pump−probe spectra proportional to $(\mu_t)^4$ is higher than in the linear IR absorption spectra proportional to $(\mu_t)^2$. The enhanced absorption below 3340 cm^{-1} is due to the $\nu = 1-2$ absorption of the two normal modes. Figure 2b shows the time-resolved bleach recovery at $\nu(NH_2)_S = 3413$ cm^{-1} and excited-state absorption decay measured at 3321 cm^{-1}, which display a similar time evolution. From an exponential fit (solid lines), we derive a $\nu = 1$ lifetime of the $\nu(NH_2)_S$ mode of $T_1 = 6 \pm 1$ ps. The time-resolved bleach recovery at 3526 cm^{-1} (not shown) gives a T_1 =10 ± 2 ps for the $\nu(NH_2)_A$ mode. Comparable values for the vibrational lifetime of N−H stretching modes have been found for other heterocyclic compounds having free N−H modes in chloroform solution.[12,30,31] There is a weak residual bleaching signal on the (fundamental) $\nu = 0-1$ transitions of $\nu(NH_2)_S$ and $\nu(NH_2)_A$, which we assign to a vibrationally heated ground state formed after the decay of the $\nu = 1$ states.

The oscillatory component on the pump−probe transients of Figure 2b, obtained after correction for the slow picosecond exponential population decay, is shown in Figure 2c,d, and the corresponding Fourier transforms are given in Figure 2e,f. From this analysis, we derive an oscillation frequency of 112 cm^{-1} (corresponding to a period of 298 fs), with a dephasing time of ∼1 ps. The pump spectrum covers both the $\nu = 0-1$ transitions of the $\nu(NH_2)_S$ and $\nu(NH_2)_A$ modes. An excitation scheme where spectrally distinct components of the pump field induce the two transitions simultaneously generates a coherent superposition of quantum states. As a result, the coherent superpositions induced by the pump pulse result in quantum beats between the $\nu(NH_2)_S$ and $\nu(NH_2)_A$ normal modes with a frequency of $2|J_H| = \nu(NH_2)_A - \nu(NH_2)_S = 112$ cm^{-1} in the subsequent time period.[32] The relatively long dephasing time of this quantum beat is fully in line with the observed difference in line widths of the inhomogeneously broadened transitions of the $\nu(NH_2)_S$ and $\nu(NH_2)_A$ modes (fwhm = 21 and 30 cm^{-1}, respectively).

Figure 3 shows 2D-IR spectra of A dissolved in $CHCl_3$, obtained with the $(k_1,k_2,k_3,k_{LO}) = (ZZYY)$ polarization

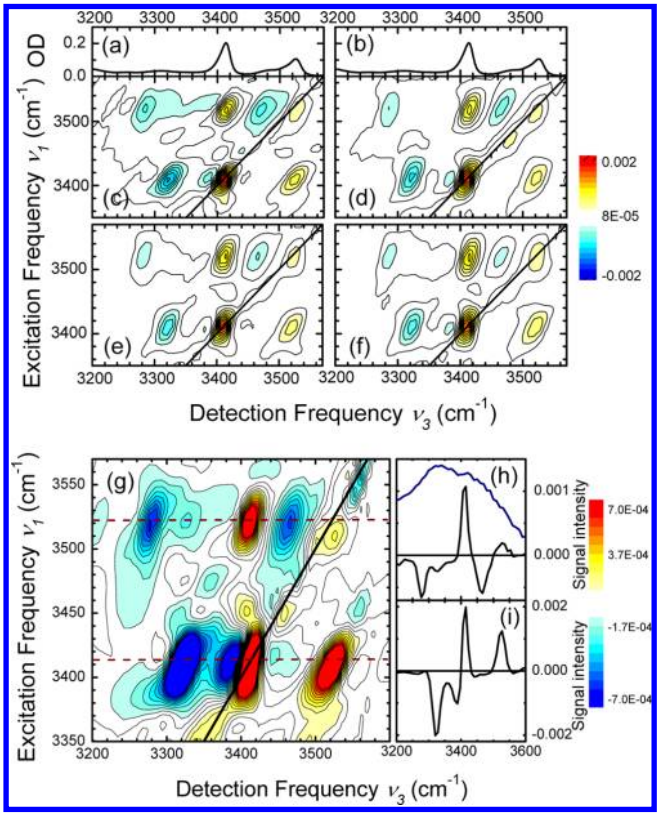

Figure 3. 2D-IR spectra of adenosine monomer as a function of the waiting time T, using the $(ZZYY)$ polarization condition: (c) 0.2, (d) 0.3, (e) 0.5, and (f) 1.0 ps. The linear FT-IR spectra are shown in the top panels (a,b). The 2D-IR spectrum measured at $T = 0.2$ ps is shown on a blown-up scale in panel (g) together with cross cuts (solid lines) for (h) $\nu_3 = 3525$ cm^{-1} and (i) $\nu_3 = 3525$ cm^{-1}. The blue line indicates the laser spectrum of the IR pulses used.

dx.doi.org/10.1021/jp303864m | J. Phys. Chem. A 2012, 116, 7636−7644

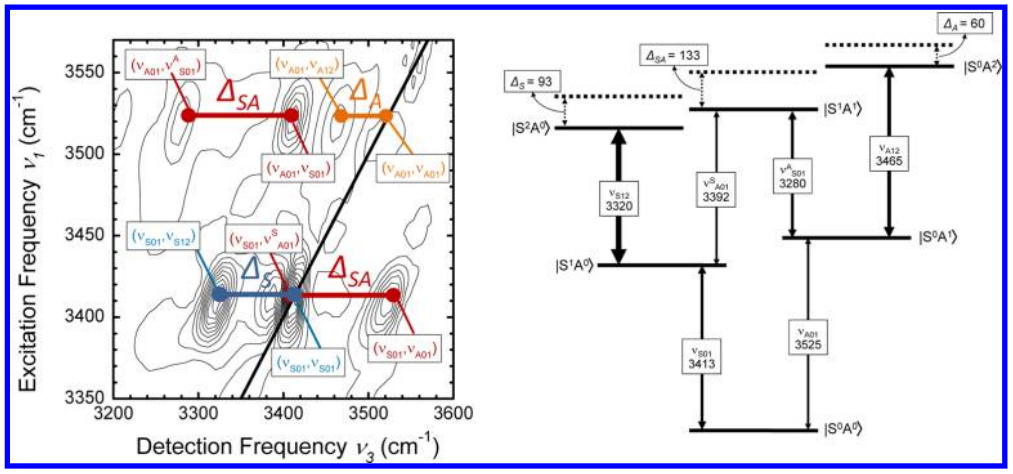

Figure 4. The level scheme in the normal mode representation is shown together with the strongly allowed $n = 0 \rightarrow 1$ and $1 \rightarrow 2$ transitions, together with the anharmonic frequency shifts for the $n = 2$ excitation manifold.

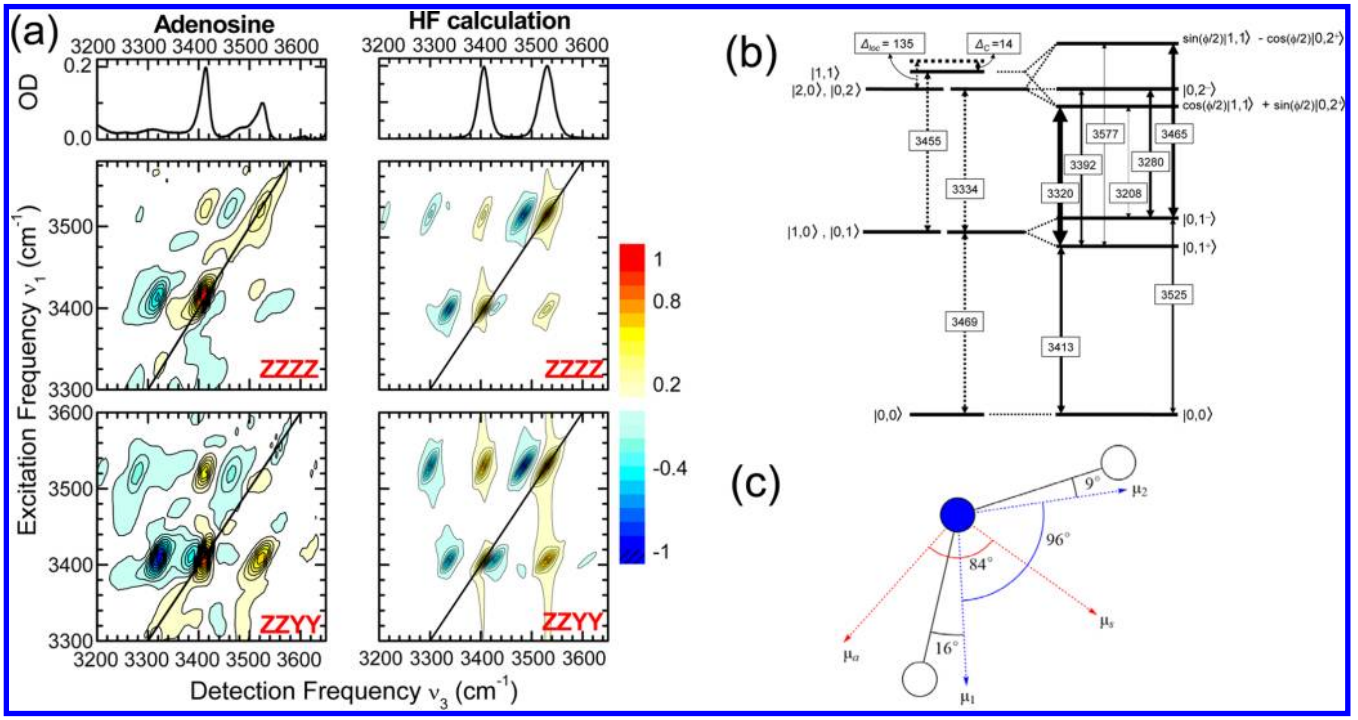

Figure 5. (a) 2D-IR spectra of the adenosine monomer (left column) recorded at a population waiting time of 200 fs, using the (*ZZZZ*) and (*ZZYY*) polarization conditions (second and third rows, respectively). Calculated 2D-IR spectra for the A monomer are given in the second column. The linear FT-IR spectra are depicted in the top panels. (b) Level scheme in the local mode representation with the uncoupled levels shown on the left and the coupled levels on the right. The thicknesses of the $n = 0 \rightarrow 1$ and $n = 1 \rightarrow 2$ transitions are scaled to the intensities in the 2D-IR spectra calculated with the coupled local mode model. (c) Orientational information on bond vectors and dipole moments.

geometry. We plot absorptive 2D-IR spectra, that is, the sum of the rephasing and nonrephasing signals. The 2D spectra were recorded for (population) waiting times of (c) $T = 0.2$, (d) 0.3, (e) 0.5, and (f) 1.0 ps. Each 2D spectrum is normalized to the maximum positive signal at $(\nu_1[\text{cm}^{-1}],\nu_3[\text{cm}^{-1}]) = (3413,3413)$. The 2D spectra display two prominent positive diagonal peaks at (3413,3413) and (3525,3525), which originate from the $\nu = 0$ to 1 transitions of the $\nu(NH_2)_S$ and $\nu(NH_2)_A$ normal modes (cf., linear infrared spectra in Figure 3a,b). In addition, there are positive cross peaks at (3413,3525) and (3525,3413) and negative off-diagonal peaks at (3413,3320), (3413,3390), (3525,3280), and (3525,3465). As a function of population time T, the spectral positions, line shapes, and relative intensities of the different peaks display minor changes. This observation suggests a minor role of spectral diffusion on this time scale and a negligible energy transfer from the $\nu(NH_2)_A$ mode at 3525 cm^{-1} to the $\nu(NH_2)_S$ mode at 3413 cm^{-1}, as is to be expected given the 6 and 10 ps lifetimes.

In Figure 3g, we show the spectrum of Figure 3c on a magnified intensity scale. Cuts along the detection frequency axis for ν_1 = 3525 and 3413 cm^{-1} (dashed lines in Figure 3g) are plotted in Figure 3h,i, together with the (intensity) spectrum of the femtosecond infrared pulses in Figure 3h. In addition to the strong peaks originating from the monomeric

dx.doi.org/10.1021/jp303864m | J. Phys. Chem. A 2012, 116, 7636−7644

species A, there are a number of weaker peaks caused by complexed molecules.

We now interpret the 2D spectra by assigning the different peaks to different vibrational transitions in the normal mode picture. The corresponding level scheme is shown in Figure 4, together with a schematic 2D spectrum including the assignments. The fundamental $\nu = 0-1$ transitions of $\nu(NH_2)_S$ and $\nu(NH_2)_A$ give rise to the diagonal peaks at $(\nu_{S01},\nu_{S01}) = (3413, 3413)$ and $(\nu_{A01},\nu_{A01}) = (3525,3525)$. In addition, there are the $\nu = 1-2$ transitions of each of the two normal modes and the transition to the combination state in which both modes are excited on their fundamental transition. The frequency spacing of the positive peak at $(\nu_{A01},\nu_{S01}) = (3525,3413)$ and the negative peak at $(\nu_{A01},\nu^{S}_{A12}) = (3525,3280)$ has a value of $\Delta_{SA} \approx 133$ cm^{-1}. The detection frequency spacing between the positive peak at $(\nu_{S01},\nu_{A01}) = (3413,3525)$ and the negative peak at $(\nu_{S01},\nu^{A}_{S01}) = (3413,3392)$ has the same value, within the experimental accuracy. Thus, we assign the two peak patterns to the two-quantum excitation of the coupled normal modes where both modes are excited on the fundamental transition and the combined excitation is anharmonically down-shifted by $\Delta_{SA} \approx 133$ cm^{-1} compared to the sum of the two fundamental frequencies of 3413 + 3525 = 6938 cm^{-1}. The pairs of positive and negative off-diagonal peaks at the two excitation frequencies $\nu_{S01} = 3413$ cm^{-1} and $\nu_{A01} = 3525$ cm^{-1} are characteristic for this double excitation.[33] In addition to such pairs of off-diagonal peaks, there are negative peaks at $(\nu_{S01},\nu_{S12}) = (3413,3320)$ and $(\nu_{A01},\nu_{A12}) = (3525,3465)$ that represent the $\nu = 1-2$ contributions of $\nu(NH_2)_S$ and $\nu(NH_2)_A$. From their detection frequency values, we derive diagonal anharmonicities $\Delta_S = 3413-3320 = 93$ cm^{-1} and $\Delta_A = 3525-3465 = 60$ cm^{-1}.

4. THEORETICAL ANALYSIS AND DISCUSSION

The measured 2D spectra are in qualitative agreement with the normal mode description, discussed in section 3. An alternative choice of vibrational coordinates are the local N−H stretching modes. In principle, the two types of mode descriptions lead to equivalent predictions of the observed transitions as they are linked by a mere basis set transformation. For a more detailed analysis with the help of theoretical calculations, we now introduce the local mode picture, which has been used extensively in overtone spectroscopy.[34−37] Using local modes has been shown to be advantageous in the explanation of the interplay of couplings and anharmonic shifts of overtone states of, in particular, hydrogen stretching modes. Comparison of the results obtained on the local N−H stretching modes of A with previously published data on O−H and N−H stretching modes of a variety of molecules is therefore straightforward.

In Figure 5, we show an energy level scheme appropriate for a discussion of the local mode picture. On the left-hand side, the ground state, the (degenerate) one-quantum and two-quantum states, as well as the combination tone are shown for the uncoupled local oscillators. The right-hand side of the scheme represents the coupled oscillators with arrows indicating the transitions between the single- and double-excitation manifolds and n indicating the number of excitation quanta in the system. We analyzed this level scheme with the $n = 1$ and 2 manifolds in the local mode representation[33,35−41] by adopting the symmetrized local mode basis with the elements

$$|i, j^{\pm}\rangle = \frac{1}{\sqrt{2}}(|i, j\rangle \pm |j, i\rangle) \qquad \text{for } i < j \tag{1a}$$

$$|i, i^{\pm}\rangle = |i, i\rangle \tag{1b}$$

The fundamental $n = 0 \rightarrow 1$ transitions occur at 3413 and 3525 cm^{-1}. From each of these $n = 1$ states, two excited-state $n = 1 \rightarrow 2$ absorption transitions are strongly allowed. With these excited-state absorption transitions, the energy location of the three levels in the $n = 2$ manifold can be accurately determined, 6735, 6805, and 6990 cm^{-1} (accuracy = ±5 cm^{-1}). Furthermore, realizing that the uncoupled fundamental local N−H stretching frequency is equal to 3469 cm^{-1}, we can deduce from this level scheme that the total diagonal anharmonicity in the double-excitation manifold is $(6 \times 3469 - 6735 - 6805 - 6990) = 284 \pm 13$ cm^{-1}.

Using the intermode coupling $J_H = -56.0$ cm^{-1} as input, we obtain a local mode diagonal anharmonicity of $\Delta_{loc} \approx 135$ cm^{-1}, which leaves for the diagonal anharmonic downshift of the combination mode $|1,1\rangle$ about $\Delta_c \approx 14$ cm^{-1}. The local mode anharmonicity $\Delta_{loc} \approx 135$ cm^{-1} is comparable to those of free (non-hydrogen-bonded) N−H stretching vibrations in heterocyclic nucleic bases or base model systems.[12,30,31] We note that, in contrast to Cho,[40,41] Child and Halonen[35−37] and Hamm and Zanni[33] do not introduce an anharmonic shift Δ_c for the combination level $|1,1\rangle$. The 14 cm^{-1} value obtained here suggests that this anharmonic shift is small for the N−H stretching local modes of adenosine. In fact, the value barely exceeds the error margin on the total anharmonicity for the $n = 2$ manifold.

To obtain insight into the microscopic origin of the anharmonicities and couplings of A, we now discuss results from ab initio quantum chemical calculations. The HF/6-311++G** potential energy surface was expanded to sixth order in the two local N−H stretching coordinates.[42,43]

$$\begin{aligned} H = {} & \sum_i \frac{p_i^2}{2m_i} + \sum_{ij} \frac{1}{2} G_{ij} p_i p_j + V_0 + \sum_i f_i r_i + \frac{1}{2!} \sum_{ij} f_{ij} r_i r_j \\ & + \frac{1}{3!} \sum_{ijk} f_{ijk} r_i r_j r_k + \frac{1}{4!} \sum_{ijkl} f_{ijkl} r_i r_j r_k r_l \\ & + \frac{1}{5!} \sum_{ijklm} f_{ijklm} r_i r_j r_k r_l r_m + \frac{1}{6!} \sum_{ijklmn} f_{ijklmn} r_i r_j r_k r_l r_m r_n \end{aligned} \tag{2}$$

where G_{ij} are elements of the Wilson G matrix[44,45] and $f^{(n)}_{k1k2...kn}$ are the nth order force constants

$$f^{(n)}_{k1k2\ldots kn} = \left(\frac{\partial^n V}{\partial r_{k1} \partial r_{k2} \ldots \partial r_{kn}} \right)_0 \tag{3}$$

The nuclear dipole moment was truncated at linear order

$$\mu = \mu_0 + \sum_i \left(\frac{\partial \mu}{\partial r_i} \right)_0 r_i \tag{4}$$

The equilibrium force constants and transition dipole moments were determined by least-squares fits to the computed potential energy surface and electric dipole, respectively. The optimized geometry agrees well with previous results.[46] The NH_2 group is roughly 10° out of plane with respect to the ring. The potential energy surface and the electric dipole moment were calculated on a grid whose points are displacements from equilibrium ranging from −0.2 to 0.2 Å in steps of 0.05 Å.

The Hamiltonian can be written in an equivalent form by transforming the internal coordinates using

$$r_i = \sqrt{\frac{\hbar}{2m_i\omega_i}}\,(B_i + B_i^\dagger) \tag{5a}$$

$$p_i = \mathrm{i}\sqrt{\frac{\hbar m_i\omega_i}{2}}\,(B_i^\dagger - B_i) \tag{5b}$$

where B_i and $B_i^\dagger$ are the bosonic annihilation and creation operators, which satisfy the commutation relation $[B_i, B_j^\dagger] = \delta_{ij}$. Using these relations, the Hamiltonian can now be written as

$$\begin{aligned} H = {} & -\frac{1}{2}\sum_{i\neq j}\gamma'_{ij}(B_i^\dagger - B_i)(B_j^\dagger - B_j) + V_0 \\ & + \sum_i g_i(B_i^\dagger + B_i) + \frac{1}{2}\sum_{i=j}\omega_i(B_i^\dagger + B_i)^2 \\ & + \frac{1}{2}\sum_{i\neq j}\varphi_{ij}(B_i^\dagger + B_i)(B_j^\dagger + B_j) \\ & + \frac{1}{3!}\sum_{ijk} g_{ijk}(B_i^\dagger + B_i)(B_j^\dagger + B_j)(B_k^\dagger + B_k) \\ & + \frac{1}{4!}\sum_{ijkl} g_{ijkl}(B_i^\dagger + B_i)(B_j^\dagger + B_j)(B_k^\dagger + B_k)(B_l^\dagger + B_l) \\ & + \frac{1}{5!}\sum_{ijklm} g_{ijklm}(B_i^\dagger + B_i)(B_j^\dagger + B_j)(B_k^\dagger + B_k) \\ & (B_l^\dagger + B_l)(B_m^\dagger + B_m) + \frac{1}{6!}\sum_{ijklmn} g_{ijklmn}(B_i^\dagger + B_i) \\ & (B_j^\dagger + B_j)(B_k^\dagger + B_k)(B_l^\dagger + B_l)(B_m^\dagger + B_m)(B_n^\dagger + B_n) \end{aligned} \tag{6}$$

where the dimensionless force constants are related to those in eq 2 by $g^{(n)}_{k1k2...kn} = [\hbar^n/(2m_{k1}\omega_{k1}2m_{k2}\omega_{k2}...2m_{kn}\omega_{kn})]^{1/2} f^{(n)}_{k1k2...kn}$. m_{kx} and ω_{kx} are the reduced mass and harmonic local mode frequency of the internal coordinate r_{kx}. The bilinear ("mechanical") coupling, which causes the splitting between the symmetric and asymmetric fundamentals, includes both a kinetic (γ'_{12}) and potential energy (φ_{12}) contribution[44,45]

$$\gamma_{12} = \gamma'_{12} - \varphi_{12} = -\frac{\sqrt{\omega_1\omega_2}\,G_{12}}{2\sqrt{G_{11}G_{22}}} - \frac{\sqrt{\omega_1\omega_2}f_{12}}{2\sqrt{f_{11}f_{22}}} \tag{7}$$

where γ'_{12} is the kinetic energy contribution and φ_{12} is the potential energy contribution. The observed splitting for 9-mA is dominated by γ'_{12} rather than φ_{12} (Table 2). The vibrational eigenstates were obtained by diagonalizing the Hamiltonian (eq 6) in a harmonic basis, which was truncated at 15 quanta (136 basis states).

The calculated anharmonic energy levels and the expansion coefficients of the Hamiltonian for 9-mA and 9-mA-d_2 are listed in Tables 1 and 2. All frequencies and anharmonicities are scaled by a factor of 0.9183. This factor, which is greater than the standard harmonic scaling factor[47] and less than the recently determined anharmonic scaling factor, based on second-order vibrational perturbation theory calculations,[48,49] was chosen to match with experiment. The calculated anharmonic energy levels match qualitatively with the anharmonicity parameters derived from the 2D-IR experiments (Figure 4). Due to the negative bilinear coupling, the symmetric stretch is lower in energy than the asymmetric stretch, as previously assigned.[6,8,26−29] Upon isotopic substitution, γ'_{12} increases by a factor of $\sqrt{2}$, which explains the greater splitting in 9-mA-d_2. A similar effect has recently been observed for water.[50]

Table 1. Comparison of Calculated and Experimentally Determined Fundamental Frequencies and Anharmonic Shifts of 9-mA in cm^{-1}[a]

	experiment	HF/6-311+G**
ν_a	3525	3530 (2861)
ν_s	3413	3406 (2704)
Δ_{aa}	60	46 (31)
Δ_{ss}	93	69 (35)
Δ_{as}	133	106 (68)
Δ_{tot}	284	219 (134)
Δ_{loc}	135	107 (65)
Δ_c	14	6 (5)

[a]Values for 9-MA-d_2 are given in parentheses.

Table 2. Anharmonic Expansion Coefficients[a] of 9-mA in cm^{-1}[b]

g_1	−0.2 (−0.2)	g_{11111}	−140.1 (−64.0)
g_2	−0.1 (−0.1)	g_{11112}	14.9 (6.8)
ω_1	3901.8 (2851.0)	g_{11122}	22.6 (10.3)
ω_2	3900.7 (2850.2)	g_{11222}	22.9 (10.4)
γ_{12}'	64.6 (88.3)	g_{12222}	15.1 (6.9)
φ_{12}	−6.7 (−4.9)	g_{22222}	−140.1 (−64.0)
g_{111}	−816.2 (−509.8)	g_{111111}	58.4 (22.8)
g_{112}	6.6 (4.1)	g_{111112}	−8.2 (−3.2)
g_{122}	5.9 (3.7)	g_{111122}	−24.2 (−9.4)
g_{222}	−815.8 (−509.6)	g_{111222}	−23.7 (−9.2)
g_{1111}	319.6 (170.7)	g_{112222}	−24.5 (−9.5)
g_{1112}	−17.4 (−9.3)	g_{122222}	−8.4 (−3.3)
g_{1122}	−13.5 (−7.2)	g_{222222}	58.5 (22.8)
g_{1222}	−17.3 (−9.2)		
g_{2222}	319.4 (170.6)		

[a]The force constants are listed as $g_{k1k2...kn} = [\hbar^n/(2m_{k1}\omega_{k1}2m_{k2}\omega_{k2}...2m_{kn}\omega_{kn})]^{1/2} f^{(n)}_{k1k2...kn}$. [b]Values for 9-MA-$d_2$ are given in parentheses.

The intensity ratio R of the symmetric and asymmetric peaks in the linear absorption spectrum (Figure 1) is estimated at ~1.45 ± 0.2. Regarding these modes as positive and negative linear combinations of N−H local modes, the angle θ between the local mode transition dipoles is predicted from $\cos\theta = (R-1)/(R+1)$ to be ~79 ± 4°. Our ab initio calculations produce an angle between the local mode transition dipoles of 95°, which confirms that the N−H stretching local mode dipoles are not parallel to the bond vectors (Figure 5). This is similar to the amide I mode, where the transition dipole moment makes a 20° angle with the C═O bond vector.[51] The angle between the symmetric and asymmetric transition dipoles is 84°.

Figure 5 compares the measured and calculated 2D-IR spectra for $(k_1,k_2,k_3,k_{LO}) = (ZZZZ)$ and $(ZZYY)$ polarization geometries. The nearly perpendicular orientation of the two transition dipole moments is reflected in the relative intensities of the cross peaks compared to those of the diagonal peaks in the 2D-IR spectra for these polarization geometries.[52] The local mode diagonal anharmonicity, Δ_{loc}, was calculated by expanding eq 2 in one dimension and calculating the resulting anharmonic shift. A comparison of the ab initio results to the

dx.doi.org/10.1021/jp303864m | J. Phys. Chem. A 2012, 116, 7636−7644

experimental parameter values derived using the coupled local mode model is shown in Table 1. Our calculations confirm that the total diagonal anharmonicity is dominated by Δ_{loc}, while Δ_c is small. Whereas the main features observed in the experiments are reproduced in the calculated 2D-IR spectra, the absolute value of the total diagonal anharmonicity, a measure of the three anharmonic shifts, is underestimated by a factor of 1.3, resulting in smaller spectral shifts of peaks in the 2D-IR spectra related to excited-state $n = 1 \rightarrow 2$ absorption transitions. The relative magnitudes of the three anharmonic shifts are roughly equal to the experimentally measured values, suggesting that a further refinement of the calculations should point at a better estimation of the N−H stretching anharmonicities.

We now discuss our findings on the diagonal anharmonicities and couplings of the N−H stretching modes of A, relating to previously reported work on hydrogen stretching oscillators, as well as indicating the repercussions that the obtained parameter values have on the fundamental $n = 0 \rightarrow 1$ and excited-state $n = 1 \rightarrow 2$ absorption transitions. It has been shown that for hydrogen stretching overtone states with $n = 2-5$ molecules, such as H_2O and C_2H_2, quenching of the intermode J_H coupling by the anharmonicity of the individual bond potentials Δ_{loc} causes a localization of vibrational excitation, that is, a local mode representation provides a better description for the experimentally determined frequency shifts of these overtone transitions.[34,35,37,53] For C_2D_2 and SO_2, the normal mode picture is more beneficial to describe the observed features. Child and Halonen[35−37] have provided the formalism to connect the local mode and normal mode representations. Depending on the relative magnitudes of coupling $J_H = -56$ cm^{-1} and diagonal anharmonicity Δ_{loc}, it follows which mode description is closer to the real situation for the overtone states. In particular, when the value of the parameter ξ, defined as:

$$\xi = \frac{2}{\pi}\arctan\left(\frac{2J}{\Delta_{loc}}\right) \tag{8}$$

is close to zero, the local mode limit applies (i.e., $|J| \ll \Delta_{loc}$). In contrast, when ξ becomes equal to ± 1, that is when $|J| \gg \Delta_{loc}$, the normal mode limit is reached. For the A monomer, with $J_H = -56$ cm^{-1} and $\Delta_{loc} = 135$ cm^{-1}, we find $\xi = -0.44$, indicating that the character of the N−H stretching modes of A in overtone states is intermediate between local and normal limits. The characteristics of the N−H stretching modes of the A monomer can at best be compared with the O−H stretching modes of gas-phase H_2O, with $\xi = -0.34$, where similar diagonal anharmonicities and couplings have been derived using the local mode picture.[35−37,53] The local mode basis has also been applied in the interpretation of overtone spectra of amines and anilines.[54,55] From such studies, it has been derived that for aliphatic amines such as methylamine and cyclopropylamine $|J_H| = 32$ cm^{-1} and $\Delta_{loc} = 158$ cm^{-1}.[55,56] For aromatic amines such as aniline, where the resonance between the nitrogen lone pair and the π-molecular orbitals leads to a planarization of the NH_2 group, the local mode coupling increases to $|J_H| = 43.65$ cm^{-1} and $\Delta_{loc} = 163.4$ cm^{-1}.[54] Comparing these literature values with those that we have found for the A monomer suggests that the magnitude of the local mode coupling increases upon increased interaction of the nitrogen lone pair with an extended aromatic π-molecular orbital system, whereas the magnitude of the local diagonal anharmonicity remains similar. To validate this, N−H stretching parameters for other molecular systems having the NH_2 functionality should be investigated.

The coupling $J_H = -56.0$ cm^{-1} leads to strong mixing of the resonant $\nu = 1$ states of the two local modes (i.e., $|J_H| \gg |\omega_1 - \omega_2| = 0$), and therefore, the normal modes are the proper eigenstates in the $n = 1$ manifold and, thus, the strong coupling regime applies to the single-excitation manifold.[33,41] In the double-excitation manifold, on the other hand, the $|1,1\rangle$ local mode state is coupled to the local mode states $|0,2\rangle$, $|2,0\rangle$ that are both lowered by the large diagonal anharmonicity Δ_{loc}. Transforming the basis set to $|1,1\rangle$, $|0,2^+\rangle$, and $|0,2^-\rangle$ eliminates the coupling between $|0,2^-\rangle$ and the other two states and produces a modified coupling of $2J_H$ between $|1,1\rangle$ and $|0,2^+\rangle$, with uncoupled energies of $2\omega_0 - \Delta_c$ and $2\omega_0 - \Delta_{loc}$, respectively. Thus, in the double-excitation manifold, the symmetric stretch overtone is only a proper eigenmode if $(\Delta_{loc} - \Delta_c)/2|J_H| \gg 1$. In the present case, this ratio is $(135 - 14)/(2 \times 56) \approx 1.1$; therefore, clearly, the intermediate coupling regime applies to the double-excitation manifold, and neither the local nor the normal mode representations provide an accurate description of these vibrational overtone eigenstates. As a result, the $|1,1\rangle$ and $|0,2^+\rangle$ states of A are strongly mixed (see Figure 5), with the mixing angle ϕ defined as

$$\phi = \arctan\left(\frac{4J}{\Delta_{loc} - \Delta_c}\right) \tag{9}$$

Finding $\phi = 118°$ for A, such strong mixing results also in the weak allowance of the harmonically forbidden three-quantum transitions. Even though in our 2D-IR experimental data sets we find indications of these forbidden transitions becoming weakly allowed, which would lead to negative cross peaks located at (3525,3210) and (3413,3575), the minute signal strengths are just above detection threshold and of similar magnitude as peaks due to A complexes, preventing us from making definitive statements on this. The calculated 2D-IR spectra indicate that the magnitudes of these additional cross peaks are within a few percent of the main peaks. Such behavior of "forbidden" transitions having small cross sections has been observed before for the excited-state $n = 1 \rightarrow 2$ transitions in 2D-IR spectra obtained on the C≡O stretching modes of $Rh(CO)_2(C_5H_7O_2)$ (I) complexes.[42,57−59] For such complexes with carbonyl stretching modes, however, $\Delta_{loc} \approx |J|$, and mixing between the symmetric stretching overtone and the combination state is less pronounced with concomitant weaker cross sections for these "forbidden" transitions.

Therefore, we feel that such rich effects of vibrational spectroscopy can be grasped best on hydrogen stretching oscillators, that is, C−H, N−H, and O−H stretching modes, with additional features that may take place upon formation of hydrogen bonds. Here, ultrafast 2D-IR spectroscopy provides a clear alternative to overtone spectroscopy to obtain direct insight into these vibrational coupling effects for molecules in the condensed phase. With ultrafast 2D-IR spectroscopy, one not only discerns the information on vibrational frequency shifts and band intensities into two spectral dimensions (as opposed to overtone spectroscopy where the transitions are recorded in one dimension), but additional orientational degrees of freedom can be explored using the polarization properties of the femtosecond IR laser pulses. A difference between the N−H and O−H stretching modes is the typically much larger spectral broadening for O−H stretching modes upon formation of hydrogen bonds, a consequence of a larger

susceptibility of O−H stretching modes to fluctuations imposed by the surrounding solvent shells.[60,61] Dynamical decoupling effects may then be expected to hinder a full determination of the interplay between coupling and diagonal anharmonicities. As a result, full characterization of the rich spectral structure of the nonlinear 2D-IR spectra is likely to happen for N−H stretching manifolds of hydrogen-bonded nucleobase pairs rather than for O−H stretching bands of hydrogen-bonded topographies consisting of multiple OH groups.

5. CONCLUSIONS

We have investigated the linear FT-IR and nonlinear femtosecond 2D-IR spectra of the N−H stretching modes of the adenosine (A) monomer in chloroform solution. On the basis of the frequency positions of the symmetric and asymmetric NH_2 stretching, of symmetric and asymmetric ND_2 stretching, and of the N−H and N−D stretching modes of NHD groups, couplings $J_H = -56$ cm^{-1} and $J_D = -77$ cm^{-1} were found. We have applied the local mode representation to fully explore the first $n = 1$ and second $n = 2$ excitation manifolds using the formalism developed to describe results from overtone spectroscopy of stretching oscillators. Whereas the local N−H stretching modes of A are degenerate in frequency, that is, $|J_H| \gg |\omega_1 - \omega_2| = 0$, making them strongly coupled in the $n = 1$ single excited states, and the symmetric and asymmetric normal modes are proper eigenmodes of the molecular system, the large local diagonal anharmonicity $\Delta_{loc} \approx 135$ cm^{-1} leads to a distinctly different behavior for the $n = 2$ double-excitation manifold, where intermediate coupling leads to the situation that neither local nor normal modes are the appropriate eigenmodes for A. We anticipate that the analysis presented here can be further refined when comparing 2D-IR spectra of N−H stretching modes in the A monomer with N−D stretching modes of deuterated A monomer, as well as extending to linear and 2D-IR spectroscopy on hydrogen-bonded A.

AUTHOR INFORMATION

Corresponding Author

*E-mail: nibberin@mbi-berlin.de.

Notes

The authors declare no competing financial interest.

ACKNOWLEDGMENTS

The research leading to these results has received funding from the European Research Council under the European Union's Seventh Framework Programme (FP7/2007-2013/ERC Grant Agreement N° 247051; T.E.), the German Science Foundation (Deutsche Forschungsgemeinschaft; F.T.), the National Institutes of Health (Grants GM059230 and GM091364; S.M.), as well as the National Science Foundation (Grant CHE-1058791; S.M.). N.K.P. is supported by a National Science Foundation Graduate Research Fellowship. We cordially acknowledge assistance in the pump−probe experiments by Dr. Ismael A. Heisler.

REFERENCES

(1) Szyc, Ł.; Yang, M.; Nibbering, E. T. J.; Elsaesser, T. *Angew. Chem., Int. Ed.* **2010**, *49*, 3598.
(2) Yang, M.; Szyc, Ł.; Elsaesser, T. *J. Phys. Chem. B* **2011**, *115*, 1262.
(3) Yang, M.; Szyc, Ł.; Elsaesser, T. *J. Phys. Chem. B* **2011**, *115*, 13093.
(4) Nir, E.; Kleinermanns, K.; de Vries, M. S. *Nature* **2000**, *408*, 949.
(5) Plützer, C.; Hünig, I.; Kleinermanns, K.; Nir, E.; de Vries, M. S. *ChemPhysChem* **2003**, *4*, 838.
(6) Dong, F.; Miller, R. E. *Science* **2002**, *298*, 1227.
(7) de Vries, M. S.; Hobza, P. *Annu. Rev. Phys. Chem.* **2007**, *58*, 585.
(8) Biemann, L.; Haber, T.; Maydt, D.; Schaper, K.; Kleinermanns, K. *J. Chem. Phys.* **2008**, *128*, 195103.
(9) Biemann, L.; Haber, T.; Kleinermanns, K. *J. Chem. Phys.* **2009**, *130*, 125102.
(10) Schwalb, N. K.; Temps, F. *J. Am. Chem. Soc.* **2007**, *129*, 9272.
(11) Schwalb, N. K.; Michalak, T.; Temps, F. *J. Phys. Chem. B* **2009**, *113*, 16365.
(12) Yang, M.; Szyc, L.; Rottger, K.; Fidder, H.; Nibbering, E. T. J.; Elsaesser, T.; Temps, F. *J. Phys. Chem. B* **2011**, *115*, 5484.
(13) Krummel, A. T.; Mukherjee, P.; Zanni, M. T. *J. Phys. Chem. B* **2003**, *107*, 9165.
(14) Krummel, A. T.; Zanni, M. T. *J. Phys. Chem. B* **2006**, *110*, 24720.
(15) Krummel, A. T.; Zanni, M. T. *J. Phys. Chem. B* **2006**, *110*, 13991.
(16) Lee, C.; Cho, M. *J. Chem. Phys.* **2006**, *125*, 114509.
(17) Lee, C.; Park, K. H.; Cho, M. *J. Chem. Phys.* **2006**, *125*, 114508.
(18) Lee, C.; Park, K. H.; Kim, J. A.; Hahn, S.; Cho, M. *J. Chem. Phys.* **2006**, *125*, 114510.
(19) Lee, C.; Cho, M. H. *J. Chem. Phys.* **2007**, *126*, 145102.
(20) Krishnan, G. M.; Kühn, O. *Chem. Phys. Lett.* **2007**, *435*, 132.
(21) Yan, Y. A.; Krishnan, G. M.; Kühn, O. *Chem. Phys. Lett.* **2008**, *464*, 230.
(22) Peng, C. S.; Jones, K. C.; Tokmakoff, A. *J. Am. Chem. Soc.* **2011**, *133*, 15650.
(23) Frisch, M. J.; Trucks, G. W.; Schlegel, H. B.; Scuseria, G. E.; Robb, M. A.; Cheeseman, J. R.; Scalmani, G.; Barone, V.; Mennucci, B.; Petersson, G. A.; Nakatsuji, H.; Caricato, M.; Li, X.; Hratchian, H. P.; Izmaylov, A. F.; Bloino, J.; Zheng, G.; Sonnenberg, J. L.; Hada, M.; Ehara, M.; Toyota, K.; Fukuda, R.; Hasegawa, J.; Ishida, M.; Nakajima, T.; Honda, Y.; Kitao, O.; Nakai, H.; Vreven, T.; Montgomery, J. A., Jr.; Peralta, J. E.; Ogliaro, F.; Bearpark, M.; Heyd, J. J.; Brothers, E.; Kudin, K. N.; Staroverov, V. N.; Kobayashi, R.; Normand, J.; Raghavachari, K.; Rendell, A.; Burant, J. C.; Iyengar, S. S.; Tomasi, J.; Cossi, M.; Rega, N.; Millam, J. M.; Klene, M.; Knox, J. E.; Cross, J. B.; Bakken, V.; Adamo, C.; Jaramillo, J.; Gomperts, R.; Stratmann, R. E.; Yazyev, O.; Austin, A. J.; Cammi, R.; Pomelli, C.; Ochterski, J. W.; Martin, R. L.; Morokuma, K.; Zakrzewski, V. G.; Voth, G. A.; Salvador, P.; Dannenberg, J. J.; Dapprich, S.; Daniels, A. D.; Farkas, Ö.; B., F. J.; V., O.; Cioslowski, J.; Fox, D. J. *Gaussian 09*, revision A.1; Gaussian, Inc.: Wallingford, CT, 2009.
(24) Mukamel, S. *Principles of Nonlinear Optical Spectroscopy*; Oxford University Press: Oxford, U.K., 1995; Vol. *6*.
(25) Abramavicius, D.; Palmieri, B.; Voronine, D. V.; Sanda, F.; Mukamel, S. *Chem. Rev.* **2009**, *109*, 2350.
(26) Plützer, C.; Nir, E.; de Vries, M. S.; Kleinermanns, K. *Phys. Chem. Chem. Phys.* **2001**, *3*, 5466.
(27) Plützer, C.; Kleinermanns, K. *Phys. Chem. Chem. Phys.* **2002**, *4*, 4877.
(28) Kabeláč, M.; Plützer, C.; Kleinermanns, K.; Hobza, P. *Phys. Chem. Chem. Phys.* **2004**, *6*, 2781.
(29) Nowak, M. J.; Lapinski, L.; Kwiatkowski, J. S.; Leszczynski, J. *J. Phys. Chem.* **1996**, *100*, 3527.
(30) Woutersen, S.; Cristalli, G. *J. Chem. Phys.* **2004**, *121*, 5381.
(31) Dwyer, J. R.; Dreyer, J.; Nibbering, E. T. J.; Elsaesser, T. *Chem. Phys. Lett.* **2006**, *432*, 146.
(32) Khalil, M.; Demirdöven, N.; Tokmakoff, A. *J. Chem. Phys.* **2004**, *121*, 362.
(33) Hamm, P.; Zanni, M. *Concepts and Methods of 2D Infrared Spectroscopy*; Cambridge University Press: Cambridge, U.K., 2011.
(34) Sage, M. L.; Jortner, J. *Adv. Chem. Phys.* **1981**, *47* (Pt. 1), 293.
(35) Child, M. S.; Halonen, L. *Adv. Chem. Phys.* **1984**, *57*, 1.
(36) Child, M. S. *Acc. Chem. Res.* **1985**, *18*, 45.
(37) Halonen, L. *Adv. Chem. Phys.* **1998**, *104*, 41.
(38) Lim, M.; Hochstrasser, R. M. *J. Chem. Phys.* **2001**, *115*, 7629.
(39) Hamm, P.; Lim, M.; Hochstrasser, R. M. *J. Phys. Chem. B* **1998**, *102*, 6123.

(40) Cho, M. H. *Chem. Rev.* **2008**, *108*, 1331.
(41) Cho, M. *Two-Dimensional Optical Spectroscopy*; CRC Press: Boca Raton, FL, 2009.
(42) Moran, A. M.; Dreyer, J.; Mukamel, S. *J. Chem. Phys.* **2003**, *118*, 1347.
(43) Hayashi, T.; Mukamel, S. *J. Phys. Chem. A* **2003**, *107*, 9113.
(44) Wilson, E. B.; Decius, J. C.; Cross, P. C. *Molecular Vibrations*; Dover Publications: New York, 1980.
(45) Kjaergaard, H. G.; Garden, A. L.; Chaban, G. M.; Gerber, R. B.; Matthews, D. A.; Stanton, J. F. *J. Phys. Chem. A* **2008**, *112*, 4324.
(46) Hobza, P.; Šponer, J. *Chem. Rev.* **1999**, *99*, 3247.
(47) Merrick, J. P.; Moran, D.; Radom, L. *J. Phys. Chem. A* **2007**, *111*, 11683.
(48) Barone, V.; et al. *J. Chem. Phys.* **2005**, *122*, 224308.
(49) Johnson, R. D.; Irikura, K. K.; Kacker, R. N.; Kessel, R. *J. Chem. Theor. Comput.* **2010**, *6*, 2822.
(50) Li, F.; Skinner, J. L. *J. Chem. Phys.* **2010**, *132*, 204505.
(51) Torii, H.; Tasumi, M. *J. Chem. Phys.* **1992**, *96*, 3379.
(52) Zanni, M. T.; Ge, N.-H.; Kim, Y. S.; Hochstrasser, R. M. *Proc. Natl. Acad. Sci. U.S.A.* **2001**, *98*, 11265.
(53) Lemus, R. *J. Mol. Spectrosc.* **2004**, *225*, 73.
(54) Howard, D. L.; Robinson, T. W.; Fraser, A. E.; Kjaergaard, H. G. *Phys. Chem. Chem. Phys.* **2004**, *6*, 719.
(55) Marom, R.; Zecharia, U.; Rosenwaks, S.; Bar, I. *J. Chem. Phys.* **2008**, *128*, 154319.
(56) Niefer, B. I.; Kjaergaard, H. G.; Henry, B. R. *J. Chem. Phys.* **1993**, *99*, 5682.
(57) Golonzka, O.; Khalil, M.; Demirdöven, N.; Tokmakoff, A. *Phys. Rev. Lett.* **2001**, *86*, 2154.
(58) Golonzka, O.; Khalil, M.; Demirdöven, N.; Tokmakoff, A. *J. Chem. Phys.* **2001**, *115*, 10814.
(59) Venkatramani, R.; Mukamel, S. *J. Chem. Phys.* **2002**, *117*, 11089.
(60) Jansen, T. L. C.; Cringus, D.; Pshenichnikov, M. S. *J. Phys. Chem. A* **2009**, *113*, 6260.
(61) Knop, S.; Jansen, T. L.; Lindner, J.; Vöhringer, P. *Phys. Chem. Chem. Phys.* **2011**, *13*, 4641.